2005-02-27

The Detection Efficiency of ARTM CPM in Aeronautical Telemetry

Michael D. Rice
mdr@byu.edu

Erik Perrins

The Detection Efficiency of ARTM CPM in Aeronautical Telemetry

Erik Perrins and Michael Rice
Department of Electrical and Computer Engineering
Brigham Young University
Provo, UT 84602
esp@ee.byu.edu, mdr@ee.byu.edu

Abstract

ARTM CPM is a partial response, two-index continuous-phase modulation that was adopted as a standard in IRIG 106-04 for aeronautical telemetry. This waveform was selected because it achieves approximately three times the spectral efficiency of PCM/FM. However, the optimum receiver requires 128 real-valued matched filters and keeps track of the waveform state with a trellis of 512 states and 2048 branches. Various complexity reducing techniques are applied and the resulting loss in detection efficiency is quantified. It is shown that the full 512-state trellis is not required to achieve the desired detection efficiency: two different 32-state configurations were found to perform within 0.05 dB of optimal; two different 16-state configurations were found to perform within 1.0 dB of optimal; and an 8-state configuration was found to perform within 1.05 dB of optimal. The analysis and simulation results show that to achieve a given state complexity, proper combination of two or more complexity-reducing techniques generally outperforms the use of a single complexity-reducing technique.

Index Terms

Continuous Phase Modulation, Aeronautical Telemetry, Maximum Likelihood Sequence Detection

I. INTRODUCTION

PCM/FM has been the dominant carrier for aeronautical telemetry since the 1970s. Spectrum reallocations of frequency bands in 1997 prompted a migration away from PCM/FM to more bandwidth efficient waveforms [1]. Size, weight, and power supply constraints force the use of fully saturated, non-linear RF power amplifiers. As a consequence, the search for more bandwidth efficient waveforms has been limited to constant envelope waveforms.

By 2004, a pair of interoperable waveforms, FQPSK [2] and SOQPSK-TG [3], were adopted in the IRIG 106 standard [4]. These waveforms achieve twice the spectral efficiency of PCM/FM even with non-linear amplifiers [5] while maintaining the same detection efficiency of PCM/FM with limiter-discriminator detection.

Recently, a partial response, multi-h CPM, denoted ARTM CPM, was adopted as part of the IRIG-106 standard [6]. This waveform achieves almost three times the spectral efficiency of PCM/FM while promising the same detection efficiency as PCM/FM with limiter-discriminator detection. The spectral improvement is realized at the expense of complexity. The optimum detector requires 128 real-valued

matched filters together with a trellis consisting of 512 states and 2048 branches. Thus, complexity reducing approximations with small decreases in detection efficiency are of tremendous importance.

This paper analyzes the performance of some well known complexity reducing techniques and quantifies the corresponding performance degradations. Some recently published techniques using an alternate representation of non-binary multi-h CPM as a parallel combination of pulse amplitude modulated (PAM) waveforms are also applied to this waveform and analyzed. It will be shown that by a proper combination of these complexity reducing techniques, a detector with 12 real-valued matched filters and a 32-state trellis with 128 branches results in a performance loss of approximately 0.01 dB.

The paper is organized as follows: The parameters of ARTM CPM and the maximum likelihood detector are described in Section II. Complexity reduction techniques are summarized and applied in Section III. These techniques are combined in Section IV where good and bad combinations are explored. The paper ends with a summary and conclusion.

II. ARTM CPM

A. Signal Model

The CPM signal may be represented as [7]

$$s(t;\boldsymbol{\alpha}) = \exp\left\{j\phi(t;\boldsymbol{\alpha})\right\} \tag{1}$$

where the phase is a pulse train of the form

$$\phi(t;\boldsymbol{\alpha}) = 2\pi \sum_i h_i \alpha_i q(t-iT) \tag{2}$$

where α_i is an M-ary symbol, T is the symbol time, h_i is the digital modulation index used during the i-th interval that cycles through a set of N_h possibilities, and $q(t)$ is the phase pulse which is usually thought of as the time-integral of a frequency pulse $f(t)$ with area 1/2. The specific values that define ARTM CPM are listed in Table I. The frequency pulse, $f(t)$, and the corresponding phase pulse $q(t)$ are plotted in Figure 1.

During the interval corresponding to the n-th symbol, $nT \le t \le (n+1)T$, the phase may be expressed as

$$\phi(t;\boldsymbol{\alpha}) = \underbrace{2\pi \sum_{i=n-2}^{n} h_i \alpha_i q(t-iT)}_{\theta(t;\boldsymbol{\alpha}_n)} + \underbrace{\pi \sum_{i=0}^{n-3} h_i \alpha_i}_{\theta_{n-3}} \tag{3}$$

where

$$\boldsymbol{\alpha}_n = \alpha_{n-2}, \alpha_{n-1}, \alpha_n \tag{4}$$

is the *correlative state vector* which contains the $L = 3$ most recent symbols. These three symbols determine the phase trajectory taken by $\theta(t; \boldsymbol{\alpha}_n)$ in (3) during the interval $nT \leq t \leq (n+1)T$. There are $M^L = 4^3 = 64$ possible values the correlative state vector can assume, each resulting in a different phase trajectory.

The second term in (3), θ_{n-3}, is called the *phase state* and represents the contribution to the carrier phase from all symbols that have worked their way through the frequency pulse and now contribute a constant value to the overall phase. Since there are two modulation indexes with values 4/16 and 5/16, it can be shown that θ_{n-3} has 32 possible values $0, \pi/16, 2\pi/16, \cdots, 31\pi/16$.

B. Maximum Likelihood Detection

Let

$$r(t) = \exp\{\phi(t; \boldsymbol{\alpha})\} + w(t) \tag{5}$$

be the received signal where $w(t)$ is a complex Gaussian random process whose real and imaginary parts are uncorrelated zero-mean random processes each with power spectral density $N_0/2$ W/Hz. The maximum likelihood estimate of the transmitted symbols is

$$\hat{\boldsymbol{\alpha}} = \arg\min_{\boldsymbol{\alpha}} \left\{ \int \left| r(t) - e^{j\phi(t;\boldsymbol{\alpha})} \right|^2 dt \right\}. \tag{6}$$

Expanding the right-hand side of this rule and ignoring terms that do not depend on the data produces an alternate, more workable form, for the decision rule:

$$\hat{\boldsymbol{\alpha}} = \arg\max_{\boldsymbol{\alpha}} \left\{ \text{Re}\left[\int r(t) e^{-j\phi(t;\boldsymbol{\alpha})} dt \right] \right\}. \tag{7}$$

The right-hand-side of (7) may be expressed recursively for use with the Viterbi Algorithm [7, Chapter 7]. At time $t = nT$ we have

$$\underbrace{\text{Re}\left[\int_0^{(n+1)T} r(t) e^{-j\phi(t;\boldsymbol{\alpha})} dt \right]}_{\lambda(n)} = \underbrace{\text{Re}\left[\int_0^{nT} r(t) e^{-j\phi(t;\boldsymbol{\alpha})} dt \right]}_{\lambda(n-1)} + \text{Re}\left[\int_{nT}^{(n+1)T} r(t) e^{-j\phi(t;\boldsymbol{\alpha})} dt \right]. \tag{8}$$

Using (3), the last term in (8) may be expressed as

$$\text{Re}\left[\int_{nT}^{(n+1)T} r(t) e^{-j\phi(t;\boldsymbol{\alpha})} dt \right] = \text{Re}\left[e^{-j\theta_{n-3}} \int_{nT}^{(n+1)T} r(t) e^{-j\theta(t;\boldsymbol{\alpha}_n)} dt \right]. \tag{9}$$

The relationships (8) and (9) suggest the receiver structure shown in Figure 2. During the interval $nT \leq t \leq (n+1)T$, the received signal is correlated with the $M^L = 64$ possible values of $\exp\{j\phi(t; \boldsymbol{\alpha})\}$ by the 64 matched filters as shown. The matched filter outputs are rotated by the possible phase states θ_{n-3}

and used to update the partial path metrics in a trellis with $32 \times M^{L-1} = 512$ states and $32 \times M^{L} = 2048$ branches. Note that each branch can be labelled with a branch vector of the form

$$\sigma = \{\theta_{n-3}, \alpha_{n-2}, \alpha_{n-1}, \alpha_n\} . \tag{10}$$

The computational requirements for the detector are summarized by the number of matched filters (or correlators) and the number of trellis states. The 64 complex-valued matched filters correspond to 256 real-valued matched filters. Half of these filters may be eliminated (through dual use) using the symmetry properties of cosine and sine. In the end, the ML detector requires 128 real-valued matched filters together with a trellis consisting of 512 states.

The probability of bit error may be quantified using the union bound with pairwise error probabilities. It was shown in [7, Chapter 2], that the probability of bit error for ML detection is

$$P_b \leq \sum_{l=0}^{\infty} C_l Q\left(\sqrt{d_l^2 \frac{E_b}{N_0}}\right) \tag{11}$$

where

$$Q(x) = \frac{1}{\sqrt{2\pi}} \int_x^{\infty} e^{-u^2/2}\ du, \tag{12}$$

E_b is the equivalent bit energy, and the constants d_l and C_l are associated with different *mergers* in the trellis. Evaluation of (11) requires knowledge of the set of distances between all possible waveforms. The distance between the waveforms corresponding to the sequences $\boldsymbol{\alpha}_1$ and $\boldsymbol{\alpha}_2$ is

$$d^2 = \frac{1}{2E_b} \int_{(R+L-1)T} \left|s(t;\boldsymbol{\alpha}_1) - s(t;\boldsymbol{\alpha}_2)\right|^2\ dt \tag{13}$$

where the difference between $\boldsymbol{\alpha}_1$ and $\boldsymbol{\alpha}_2$ is nonzero for a span of R symbols and the interval of integration corresponds to this interval. For ARTM CPM the sequences which satisfy

$$\boldsymbol{\alpha}_1 - \boldsymbol{\alpha}_2 = \ldots, 0, 2, -4, 6, -4, 2, 0, \ldots \tag{14}$$

and

$$\boldsymbol{\alpha}_1 - \boldsymbol{\alpha}_2 = \ldots, 0, 2, -2, 0, 2, -2, 0, \ldots \tag{15}$$

have the smallest two distances[1]. The coefficient C_l is given by

$$C_l = \frac{W_l N_l}{\log_2(M) N_h M^R} \tag{16}$$

[1]These two sequences differ over a span of $R = 5$ symbols. There are sequence pairs for which $R < 5$, but these sequences have larger distances.

where W_l is the the number of bit errors associated with the trellis path pairs that differ by d_l, N_l is the number of trellis path pairs that differ by d_l, and $N_h = 2$ is the number of modulation indexes. There are 72 sequence pairs that satisfy (14), have a distance $d^2 = 1.29$, and correspond to 7 bit errors. There are 648 sequence pairs that satisfy (15), have a distance of $d^2 = 1.66$, and correspond to 4 bit errors. Thus, the first two terms in (11) are

$$P_b \approx \frac{(7)(72)}{(2)(2)(4^5)} Q\left(\sqrt{1.29\frac{E_b}{N_0}}\right) + \frac{(4)(648)}{(2)(2)(4^5)} Q\left(\sqrt{1.66\frac{E_b}{N_0}}\right) \tag{17}$$

The computational burden in the detector can be reduced by proper selection of approximations that reduce the number of matched filters, trellis states, or both. Each of these complexity-reducing techniques is accompanied by an increase in the signal-to-noise ratio required to achieve a target bit error rate. The complexity/SNR trade-off is the subject of the remainder of this paper.

III. Complexity Reducing Techniques

A. Tilted Phase

The first complexity-reducing technique that can be applied is the "tilted phase" technique described by Rimoldi [8]. This method uses a different value, called the tilted phase, in place of the phase state to reduce the number of phase states by 2. The tilted phase values for ARTM CPM are

$$\tilde{\theta}_{n-3} = 0, \frac{2\pi}{16}, \ldots, 15\frac{2\pi}{16} \tag{18}$$

There is no loss in detection efficiency with this technique. By using only 16 phase states, the number of trellis branches is reduced from 2048 to 1024. The branch vector labels in this case are

$$\sigma = \left\{\tilde{\theta}_{n-3}, \alpha_{n-2}, \alpha_{n-1}, \alpha_n\right\}. \tag{19}$$

The number of matched filters required remains the same. The tilted phase is assumed for the remainder of the paper.

B. Frequency Pulse Truncation

Another complexity-reducing technique is to form a trellis based on a truncated frequency pulse of length $L'T$, where $L' \leq 3$. This technique was first proposed by Svensson, Sundberg, and Aulin [9] and a nice description can be found in [7, Chapter 8]. This approach is motivated by the observation that the amplitude of the frequency pulse in Figure 1 is very small at the ends. As an example, by approximating the frequency pulse with a length-$2T$ pulse, the phase trajectory $\theta(t; \alpha_{n-2}, \alpha_{n-1}, \alpha_n)$ is now a function of

only α_{n-1} and α_n and can be replaced by a new phase trajectory $\tilde{\theta}(t;\alpha_{n-1},\alpha_n)$. The contribution of the symbol α_{n-2} is absorbed into the phase state $\tilde{\theta}_{n-2}$. The branch vector becomes

$$\sigma = \left\{\tilde{\theta}_{n-2}, \alpha_{n-1}, \alpha_n, \right\}. \tag{20}$$

As a consequence, the number of matched filters is reduced from 128 to 32, the number of trellis phase states is reduced from 256 to 64. We point out that this reduction in states is a *correlative state reduction*, because one coordinate from the correlative state vector has been removed. The metric update equation becomes

$$\lambda(n) = \lambda(n-1) + \mathrm{Re}\left[e^{-j\tilde{\theta}_{n-2}} \int_{(n+1/2)T}^{(n+3/2)T} r(t) e^{-j\tilde{\theta}(t;\alpha_{n-1},\alpha_n)} dt\right]. \tag{21}$$

The performance analysis must account for the fact that the signal model used by the demodulator $\tilde{s}(t;\boldsymbol{\alpha})$ is different than the transmitted signal $s(t;\boldsymbol{\alpha})$. The analysis of *mismatched* detectors was introduced by Svensson, Sundberg, and Aulin [9]. It is based on the modified distance between the signals corresponding to $\boldsymbol{\alpha}_1$ and $\boldsymbol{\alpha}_2$:

$$\tilde{d} = \frac{1}{\sqrt{2E_b}} \frac{\displaystyle\int |\tilde{s}(t;\boldsymbol{\alpha}_2) - s(t;\boldsymbol{\alpha}_1)|^2 \; dt - \int |\tilde{s}(t;\boldsymbol{\alpha}_1) - s(t;\boldsymbol{\alpha}_1)|^2 \; dt}{\sqrt{\displaystyle\int |\tilde{s}(t;\boldsymbol{\alpha}_1) - \tilde{s}(t;\boldsymbol{\alpha}_2)|^2 \; dt}} \tag{22}$$

where the interval of integration is $(R + L' - 1)T$ and corresponds to the interval where $\boldsymbol{\alpha}_1$ and $\boldsymbol{\alpha}_2$ are different. The probability of error can be bounded using a union bound consisting of pairwise error probabilities based on the modified distance measure (22). The first two terms of the union used in (17) are modified to account for the variation in distances introduced by the approximation. As a result, the probability of bit error is well approximated by

$$P_b \approx \frac{7}{(2)(2)(4^5)} \sum_{k=0}^{71} Q\left(\tilde{d}_k \sqrt{\frac{E_b}{N_0}}\right) + \frac{4}{(2)(2)(4^5)} \sum_{m=0}^{647} Q\left(\tilde{d}_m \sqrt{\frac{E_b}{N_0}}\right) \tag{23}$$

where the modified distance measures are illustrated in Figure 3 (a) and (b) for $L' = 2$ and $L' = 1$, respectively. In the figure, these distance quantities are given in their squared form for easy comparison with the optimal squared distances (dashed lines in the figures). In general, however, there is no guarantee that the modified distance (22) is a positive quantity. For this reason it is used in (23) as an unsquared quantity. These plots illustrate the effect of frequency pulse truncation on performance. For $L' = 2$, there are some paths with a modified distance measure as low as 1.22 (note there are other paths with a modified distance measure of 1.37). For $L' = 1$, there are some paths with a modified distance measure as small as 0.32.

The bit error rate performance for this approximation is shown in Figure 4. Observe that the simulation results coincide with the approximation (23) for large E_b/N_0 but are different for small E_b/N_0. (This is to be expected since truncated union bounds are only accurate asymptotically.) The $L'=2$ approximation results in a very small loss, while the $L'=1$ results in a much larger loss. The performance/complexity trade-off is summarized in Table II. The $L'=2$ approximation was used in the results reported in [10].

C. Reduced State Sequence Detection (RSSD)

Reduced state sequence estimation (RSSD) was first applied to detection of partial response CPM by Svensson [11]. In the course of normal operation, the VA declares survivors at each merging node in the trellis. Each branch is labelled with a four element branch vector of the form (19). The element α_{n-2} can be replaced by its decision $\hat{\alpha}_{n-2}$, resulting in the branch vector

$$\sigma = \left\{\tilde{\theta}_{n-3}, \hat{\alpha}_{n-2}, \alpha_{n-1}, \alpha_n\right\}. \tag{24}$$

As a consequence, the number of trellis states is reduced to $16 \times 4 = 64$. This has the same effect on the trellis as frequency pulse truncation with $L'=2$. The MFs still require the three elements of the correlative state vector (4) and the number remains unchanged at 128. In the same way, α_{n-1} and α_{n-2} can be replaced by their decisions $\hat{\alpha}_{n-1}$ and $\hat{\alpha}_{n-2}$, resulting in the branch vector

$$\sigma = \left\{\tilde{\theta}_{n-3}, \hat{\alpha}_{n-2}, \hat{\alpha}_{n-1}, \alpha_n\right\}. \tag{25}$$

The number of trellis states in this case is 16 and the effect on the trellis is the same as frequency pulse truncation with $L'=1$. This type of approximation is referred to as RSSDα.

The probability of error for this detector is given by (11) where the distances are computed using (13) except L'' is used in place of L. When α_{n-2} is replaced its decision $\hat{\alpha}_{n-2}$, the metrics can only accumulate distance over an interval of $(R+2-1)T$ instead of $(R+3-1)T$. In this case $L''=2$. The squared distances for the first two terms in the union bound are 1.27 and 1.64. The probability of error is approximated by

$$P_b \approx \frac{(7)(72)}{(2)(2)(4^5)} Q\left(\sqrt{1.27\frac{E_b}{N_0}}\right) + \frac{(4)(648)}{(2)(2)(4^5)} Q\left(\sqrt{1.64\frac{E_b}{N_0}}\right). \tag{26}$$

Similarly, when both α_{n-1} and α_{n-2} are replaced by their decisions $\hat{\alpha}_{n-1}$ and $\hat{\alpha}_{n-2}$, $L''=1$. The squared distances for the first two terms in the union bound are 0.93 and 1.13. The probability of error is approximated by

$$P_b \approx \frac{(7)(72)}{(2)(2)(4^5)} Q\left(\sqrt{0.93\frac{E_b}{N_0}}\right) + \frac{(4)(648)}{(2)(2)(4^5)} Q\left(\sqrt{1.13\frac{E_b}{N_0}}\right). \tag{27}$$

The bit error rate performance for this approximation is shown in Figure 5. Observe that the simulation results coincide with the approximation (26) for large E_b/N_0. This is not so for the $L'' = 1$ case with (27). The simulation results are worse than the analysis predicts due to propagation of decision errors [11]. The performance/complexity trade-off is summarized in Table III.

Decision feedback may be applied in an entirely different manner to reduce the number of phase states in the trellis. The 16 phase states are collapsed into p' phase states using the branch vector label

$$\sigma = \left\{ \left(\frac{16}{p'} \tilde{\theta}_{n-3} \right) \bmod (2\pi), \alpha_{n-2}, \alpha_{n-1}, \alpha_n \right\}. \tag{28}$$

The actual phase information lost via the modulo operation is retained using decision feedback in the calculation of the branch metrics, as described in [11]. This type of decision feedback is referred to as RSSDθ. This technique can be applied in addition to any of the correlative state reduction techniques discussed previously.

The probability of error for this detector is given by (11) using the squared distance given by (13). The part that is different is that there are many extra terms in the union bound (11) that correspond to "rogue" mergers created by this reduced trellis. For $p' \geq 4$, these mergers have a negligible impact on the performance and the probability of bit error is well approximated by (17). When $p' = 2$ the rogue mergers have a more pronounced impact and must be taken into account. This is done by computing the distances of these rogue mergers and including additional terms from the union bound in the approximation:

$$P_b \approx \frac{(7)(72)}{(2)(2)(4^5)} Q\left(\sqrt{1.29 \frac{E_b}{N_0}} \right) + \frac{(4)(648)}{(2)(2)(4^5)} Q\left(\sqrt{1.66 \frac{E_b}{N_0}} \right) + \frac{(4)(36)}{(2)(2)(4^3)} Q\left(\sqrt{1.43 \frac{E_b}{N_0}} \right) + \frac{(4)(162)}{(2)(2)(4^4)} Q\left(\sqrt{1.53 \frac{E_b}{N_0}} \right). \tag{29}$$

The bit error rate performance for this approximation is shown in Figure 6. Observe that the simulation results coincide with the approximation (23) for large E_b/N_0 except for $p' = 2$. The simulation results are worse than the analysis predicts due to propagation of decision errors [11]. The performance/complexity trade-off is summarized in Table IV.

D. Pulse Amplitude Modulation (PAM) Technique

An entirely different viewpoint for CPM is given by the PAM representation, which was first derived for binary single-h CPM by Laruent [12] and later extended to M-ary single-h CPM by Mengali and Morelli [13] and to M-ary multi-h CPM by Perrins and Rice [14], [15]. Using the PAM representation,

the ARTM CPM waveform may be expressed as

$$s(t;\boldsymbol{\alpha}) = \sum_{k=0}^{47} \sum_{i} a_{k,i} g_{k,i}(t - iT) \tag{30}$$

where $\{a_{k,i}\}$ is a set of 48 *pseudo-symbols* which modulate the amplitude of the 48 signal pulses $g_{k,i}(t)$[2]. The details required to construct the pseudo-symbols and signal pulses are too numerous to give here, a full description is available in [15]. The essential characteristics of these quantities are

1) the signal pulses vary in amplitude and duration,
2) there is one pulse of length $4T$, 2 pulses of length $3T$, 9 pulses of length $2T$, and 36 pulses of length T,
3) the longest pulses (of duration $3T$ and $4T$) have the largest amplitude while the shortest pulses (of duration T) have extremely small amplitude,
4) the set of 48 pseudo-symbols can be represented by a 256-state trellis (using the tilted phase) with the branch vector (19), and
5) within the set of 48 pseudo-symbols, the ones associated with the largest pulses do not require a full 256-state trellis.

The most straightforward approach to complexity reduction is simply to truncate the outer sum in (30). This type of detector was described by Kaleh [16] for binary CPM and Colavolpe and Raheli [17] for non-binary CPM. The approximate signal resulting from using the first K terms is given by

$$s'(t;\boldsymbol{\alpha}) = \sum_{k=0}^{K-1} \sum_{i} a_{k,i} g_{k,i}(t - iT). \tag{31}$$

The branch metric for this detector is given by

$$\lambda(n) = \lambda(n-1) + \text{Re}\left[\sum_{k=0}^{K-1} z_{k,n} a_{k,n}^{*}\right] - S \tag{32}$$

where the sampled matched filter output is

$$z_{k,n} = \int_{nT}^{(n+D_k)T} r(t) g_{k,n}(t - nT)\ dt \tag{33}$$

and S is a constant that arises from the fact that the truncation produces approximations that no longer have the same energy. The pulses $g_{k,n}(t)$ have a duration of D_k symbol times and the shortest pulse has a duration of $D_{\min} = \min_{0<k<K-1} D_k$.

[2]There are actually 48 pulses for each modulation index. Since there are two modulation indexes, there are $2 \times 48 = 96$ pulses. But, since the modulation indexes alternate between the two possible values 4/16 and 5/16, only half of the 96 pulses are active during an interval T. For this reason, the equivalent PAM representation (30) sums 48 pulses.

As K decreases, the approximation error increases, the MF complexity decreases, and the performance decreases. The state complexity is actually determined by the *length* of the pulses used in the approximation, not by the *number* of pulses used (this non-obvious fact is demonstrated in [18]). For this reason, the truncation should include all pulses of the same length. Thus the natural choices for K are 1, 3, 12, and 48.

The mismatched detector analysis described previously is used to analyze the performance of these approximations. For the PAM case, the modified distance measure reduces to [19]

$$d' = \frac{1}{\sqrt{2E_b}} \frac{2\mathrm{Re}\int s(t;\boldsymbol{\alpha}_1)\left(s''(t;\boldsymbol{\alpha}_1)-s''(t;\boldsymbol{\alpha}_2)\right)^* \, dt + \int \left|s'(t;\boldsymbol{\alpha}_2)\right|^2 \, dt - \int \left|s'(t;\boldsymbol{\alpha}_1)\right|^2 \, dt}{\sqrt{\int \left|s''(t;\boldsymbol{\alpha}_1)-s''(t;\boldsymbol{\alpha}_2)\right|^2 \, dt}} \tag{34}$$

where $s'(t;\boldsymbol{\alpha})$ is given by (31) and $s''(t;\boldsymbol{\alpha})$ is given by

$$s''(t;\boldsymbol{\alpha}) = \sum_{k=0}^{K-1} \sum_{i=\max(N_1, n-D_k+1)}^{\min(n,N_2-1)} a_{k,i} g_{k,i}(t-iT). \tag{35}$$

which differs from (31) only in the limits of the inner sum. The first symbol index where $\boldsymbol{\alpha}_1 - \boldsymbol{\alpha}_2$ is non-zero corresponds to N_1, and $N_2 = N_1 + R + L - D_{\min}$.

The bit error probability is given by (23) by substituting $\tilde{d}$ with d'. The distances are listed in Figure 7 (a) for the $K = 1$ case in their *unsquared* form. Many of these distances have negative values, which is the root cause of the error floor observed in Figure 8. In Figure 7 (b) the *squared* distances are listed for the $K = 3$ case along with the optimal squared distances for comparison.

The bit error probability curves generated by the PAM distance measure (34) along with the simulation performance of the three approximations is illustrated in Figure 8. When $K = 1$ the approximation error is extremely large and there are paths with a negative modified distance measure. As a consequence, an error floor is observed. When $K = 3$ the losses become more acceptable, and when $K = 12$ the losses are negligible. When $K = 48$, (31) is no longer an approximation of (30) and the PAM detector becomes an alternate configuration of MLSD. The performance/complexity trade-off for these PAM detectors is summarized in Table V. The MFs are quantified in terms of real-valued length-T filters. For example, the length-$4T$ pulse requires 8 such MFs to filter the complex-valued received signal in (5).

There are other approximations for PAM-based detectors besides truncating the sum in (31). These involve averaging the original set of pulses $\{g_{k,n}(t)\}$ to produce an alternate set of pulses. We highlight two of these averaging schemes.

The first is very similar to the $K = 3$ approximation discussed above. The minimum mean-squared error approximation in [15] is applied to obtain the three pulses $p_{0,i}(t)$, $p_{1,i}(t)$, and $p_{2,i}(t)$, having durations of $4T$, $3T$, and $3T$ respectively. The approximate signal in this case is

$$s'(t;\boldsymbol{\alpha}) = \sum_{k=0}^{2} \sum_{i} a_{k,i} p_{k,i}(t - iT). \tag{36}$$

As with the $K = 3$ approximation, the pseudo-symbols associated with these pulses require a trellis of only 16 states, with branches defined by

$$\sigma = \left\{ \tilde{\theta}_{n-1}, \alpha_n, \right\}. \tag{37}$$

Observe that this trellis is the same as that of frequency pulse truncation with $L' = 1$, and RSSDα with $L'' = 1$.

The second averaging scheme is derived directly from the $K = 12$ approximation discussed above. The the number of pulses is reduced from twelve down to three by averaging the two length-$3T$ pulses to form a single pulse. Similarly, the nine length-$2T$ pulses are averaged to form a single pulse. We also average the multi-h pulses to form the equivalent of single-h pulses. The final pulses are $\overline{g}_0(t)$, $\overline{g}_1(t)$, and $\overline{g}_2(t)$, having durations of $4T$, $3T$, and $2T$ respectively. Note that the subscript i has been dropped from these pulses to reflect their single-h equivalence. The approximate signal in this case is

$$s'(t;\boldsymbol{\alpha}) = \sum_{k=0}^{2} \sum_{i} \overline{a}_{k,i} \overline{g}_k(t - iT) \tag{38}$$

where $\overline{a}_{k,i}$ are a weighted sum of the original pseudo-symbols $a_{k,i}$. The remainder of the details for this approximation are in [18]. This 3-pulse approximation, as well as the $K = 12$ approximation upon which it is based, require the 64-state trellis defined by (20).

The performance of these two averaged schemes is shown in Figure 9. Observe that the minimum mean-squared error approximation performs slightly better than the $K = 3$ approximation in Figure 8. The 3-pulse scheme with $\overline{g}_k(t)$ performs almost as well as the $K = 12$ approximation in Figure 8. The probability of bit error curves in Figure 9 are generated from the PAM distance measure in (34) by substituting the approximation respective approximation, (36) or (38), in the place of (31). The performance/complexity trade-off for these averaged PAM detectors is also summarized in Table V.

E. Orthonormal Basis Functions

There have been a number of different methods proposed to decompose CPM signals into a set of orthonormal basis functions. The most recent of these, proposed by Moqvist and Aulin [20], is highlighted

here. (For a listing of other approaches of this type, see the references in [20]). The ARTM CPM signal can be exactly represented by

$$s(t;\boldsymbol{\alpha}) = e^{j\theta_{n-3}} \sum_{j=1}^{64} c_j(\boldsymbol{\alpha}_n)\varphi_j(t-nT) \tag{39}$$

where $\{\varphi_j(t)\}$ is a set of 64 complex-valued length-T *basis functions* that span the signal space and $\{c_j(\boldsymbol{\alpha}_n)\}$ is a set of 64×64 complex-valued *projection coefficients* which map these basis functions into the 64 signals possible signals given by the correlative state vector (4). The goal of this alternate representation is to achieve a reasonably good approximation with only a limited number of basis functions. The approximate signal is given by

$$\tilde{s}(t;\boldsymbol{\alpha}) = e^{j\theta_{n-3}} \sum_{j=1}^{H} c_j(\boldsymbol{\alpha}_n)\varphi_j(t-nT) \tag{40}$$

where $H \leq 64$. This approximation does not reduce the number of trellis states, it only reduces the size of the filter bank. The metric update equation becomes

$$\lambda(n) = \lambda(n-1) + \mathrm{Re}\left[e^{-j\tilde{\theta}_{n-3}} \sum_{j=1}^{H} c_j^*(\tilde{\boldsymbol{\alpha}}_n) \int_{nT}^{(n+1)T} r(t)\varphi_j^*(t-nT)\ dt \right]. \tag{41}$$

The mismatched detector analysis is also used here to characterize the performance of these detectors. Due to the elegance of the signal space decomposition, the squared Euclidian distance between the signals corresponding to $\boldsymbol{\alpha}_1$ and $\boldsymbol{\alpha}_2$ is given by

$$\hat{d}^2 = \sum_i \sum_{j=1}^{H} |c_j(\boldsymbol{\alpha}_{i,1}) - c_j(\boldsymbol{\alpha}_{i,2})|^2 \tag{42}$$

where the outer sum is non-zero for only $R+L-1$ values of i. These distance terms are used in the same manner as (23) to yield a bit error probability.

The performance of this approximation is shown in Figure 10. The simulation results coincide with the analytical results for large E_b/N_0. The performance/complexity tradeoff is summarized in Table VI.

IV. Combined Techniques for Complexity Reduction

Table VII summarizes the properties of the complexity-reducing techniques described above in terms of whether or not they reduce the number of phase states, correlative states, and/or MFs. From the table it is clear that no single method accomplishes all three types of complexity reduction. However, the table does suggest ways in which these methods may be combined to achieve this end. For example, a frequency pulse truncation-RSSDθ combination leads to phase state reduction, correlative state reduction and MF reduction. Three such composite approaches are explored in this section.

A. Frequency Pulse Truncation and RSSDθ

It has already been established that frequency pulse truncation performs very well for $L' = 2$ and much less so for $L' = 1$. It has also been shown that RSSDθ performs very well for $p' \geq 4$. It is interesting to consider whether these results also hold when the two techniques are combined. One such combination is $p' = 8$ and $L' = 2$, which produces the 32-state trellis defined by the branch vector

$$\sigma = \left\{ \left(\frac{16}{8} \tilde{\theta}_{n-2} \right) \bmod (2\pi), \alpha_{n-1}, \alpha_n \right\}. \tag{43}$$

The performance analysis of this combination is based on the mismatched detector analysis using modified distance (22). The two mergers in (14) and (15) are sufficient to characterize the bit error performance using the truncated union bound (23).

Another configuration is $p' = 4$ and $L' = 2$, which produces the 16-state trellis defined by

$$\sigma = \left\{ \left(\frac{16}{4} \tilde{\theta}_{n-2} \right) \bmod (2\pi), \alpha_{n-1}, \alpha_n \right\}. \tag{44}$$

The bit error analysis must be expanded from the previous case to include the effect of the rogue merger $\boldsymbol{\alpha}_1 - \boldsymbol{\alpha}_2 = \ldots, 0, 2, 0, \ldots$. The rogue mergers produce 6 distinct squared distances ranging from 1.31 to 1.51. The probability of error starts with (23) and includes a third summation term to account for these rogue mergers:

$$P_b \approx \frac{7}{(2)(2)(4^5)} \sum_{k=0}^{71} Q\left(\tilde{d}_k \sqrt{\frac{E_b}{N_0}} \right) + \frac{4}{(2)(2)(4^5)} \sum_{m=0}^{647} Q\left(\tilde{d}_m \sqrt{\frac{E_b}{N_0}} \right) + \frac{1}{(2)(2)(4)} \sum_{l=0}^{5} Q\left(\tilde{d}_l \sqrt{\frac{E_b}{N_0}} \right). \tag{45}$$

The performance of these two approximations is shown in Figure 11. Observe that the $p' = 8$, $L' = 2$ combination has essentially no loss while the $p' = 4$, $L' = 2$ has a noticeable performance degradation. Thus it appears that when $L' = 2$, RSSDθ can not be applied as aggressively as when $L' = 3$. This is to be expected since the interval of integration in (22) is shortened when $L' = 2$, which makes the trellis more susceptible to rogue mergers as p' decreases. Observe that the 16-state composite detector ($L' = 4$, $p' = 8$) has a loss of only 0.80 dB, compared to the much larger loss of 4.10 dB in Table II for a 16-state detector using frequency pulse truncation alone.

B. Pulse Amplitude Modulation and RSSD

From the earlier discussion of the PAM detectors, a desirable complexity/performance tradeoff was achieved using the 3-pulse approximation with $\overline{g}_0(t)$, $\overline{g}_2(t)$, and $\overline{g}_2(t)$. This PAM approximation is now used along with RSSD. The first configuration is PAM-RSSDθ with $p' = 8$, which has the 32-state trellis

in (43). The performance analysis for this combination is based on the mismatched detector analysis using the modified distance is given by (34). The bit error probability is given by

$$P_b \approx \frac{7}{(2)(2)(4^5)} \sum_{k=0}^{71} Q\left(d'_k \sqrt{\frac{E_b}{N_0}}\right) + \frac{4}{(2)(2)(4^5)} \sum_{m=0}^{647} Q\left(d'_m \sqrt{\frac{E_b}{N_0}}\right). \tag{46}$$

The squared modified distances in the first summation range from 1.02 to 1.52 and the those in the second summation range from 1.33 to 1.96.

The second combination is PAM-RSSDθ with $p' = 4$, which has the 16-state trellis in (44). The bit error probability for this combination adds an additional term to (46) to account for the rogue mergers described previously:

$$P_b \approx \frac{7}{(2)(2)(4^5)} \sum_{k=0}^{71} Q\left(d'_k \sqrt{\frac{E_b}{N_0}}\right) + \frac{4}{(2)(2)(4^5)} \sum_{m=0}^{647} Q\left(d'_m \sqrt{\frac{E_b}{N_0}}\right) + \frac{1}{(2)(2)(4)} \sum_{l=0}^{5} Q\left(d'_l \sqrt{\frac{E_b}{N_0}}\right). \tag{47}$$

The modified distance profiles for the first two summations are the same as those in (46). The squared modified distances in the third summation range from 1.17 to 5.27.

These two cases are very similar to the previous example with frequency pulse truncation. The last configuration uses PAM-RSSDθ-RSSDα. In this case the original correlative state vector in (4) is shortened by the PAM approximation *and* RSSDα. The symbol α_{n-2} is removed by the 3-pulse PAM approximation. The symbol α_{n-1} is replaced by the decision $\hat{\alpha}_{n-1}$ via RSSDα. The 8-state trellis for this configuration is defined by the branch vector

$$\sigma = \left\{ \left(\frac{16}{8} \tilde{\theta}_{n-2} \right) \bmod (2\pi), \hat{\alpha}_{n-1}, \alpha_n \right\}. \tag{48}$$

The bit error probability for this combination is given by (46) except a different set of modified distance measures is used. The modified squared distances in the first summation range from 0.67 to 1.99 and the modified squared distances in the second summation range from 0.91 to 2.53. Note that in computing these distances (for the 8-state configuration), the value of $N_2 = N_1 + R + L - 1 - D_{\text{min}}$ must be used in (35) when computing the distance (34) to reflect the shortening of the correlative state vector via RSSDα.

The performance of these three detectors is shown in Figure 12. It is interesting to note that the composite PAM detectors perform better than the composite frequency pulse truncation detectors as the state complexity goes down. The PAM approximation has the additional advantage of having fewer MFs. The reason the PAM approximation performs well even when the correlative state vector is severely shortened is because its MFs (pulses) are longer than one symbol time [19], as shown in (33). In fact, the 8-state trellis in (48) leads to severe losses when attempted using frequency pulse truncation.

C. Orthogonal Basis Functions and RSSD

The last composite configuration to consider is the use of orthogonal basis functions with RSSDθ and RSSDα. It has already been shown that RSSDθ introduces rogue mergers, and that shortening the correlative state vector only compounds this problem. The PAM approximation has been shown to be somewhat robust against these rogue mergers since its MFs are longer. Frequency pulse truncation is also somewhat robust against rogue mergers because its branch metrics are delayed (compare the limits of integration in (9) and (21)). Neither the standard branch metric (9) or the orthogonal basis function metric (41) have such protection against rogue mergers. Therefore, it is expected that RSSDθ can not be applied as aggressively as with the PAM or frequency pulse truncation techniques.

The first configuration considered is $H = 3$, $p' = 8$, and $L'' = 2$, which has the 32-state trellis given by the branch vector

$$\sigma = \left\{ \left(\frac{16}{8} \tilde{\theta}_{n-3} \right) \bmod (2\pi), \hat{\alpha}_{n-2}, \alpha_{n-1}, \alpha_n \right\}. \tag{49}$$

The bit error probability of this technique is given by

$$P_b \approx \frac{7}{(2)(2)(4^5)} \sum_{k=0}^{71} Q\left(\hat{d}_k \sqrt{\frac{E_b}{N_0}} \right) + \frac{4}{(2)(2)(4^5)} \sum_{m=0}^{647} Q\left(\hat{d}_m \sqrt{\frac{E_b}{N_0}} \right) \tag{50}$$

where the modified distances $\hat{d}_k$ and $\hat{d}_m$ are given by (42). The squared modified distances in the first term range from 1.28 to 1.29 while those in the second term range from 1.65 to 1.66.

The second configuration is $H = 3$, $p' = 4$, and $L'' = 2$, which has the 16-state trellis given by

$$\sigma = \left\{ \left(\frac{16}{4} \tilde{\theta}_{n-3} \right) \bmod (2\pi), \hat{\alpha}_{n-2}, \alpha_{n-1}, \alpha_n \right\}. \tag{51}$$

The bit error probability of this technique starts with (50) and adds a third term to account for the rogue mergers:

$$P_b \approx \frac{7}{(2)(2)(4^5)} \sum_{k=0}^{71} Q\left(\hat{d}_k \sqrt{\frac{E_b}{N_0}} \right) + \frac{4}{(2)(2)(4^5)} \sum_{m=0}^{647} Q\left(\hat{d}_m \sqrt{\frac{E_b}{N_0}} \right) + \frac{1}{(2)(2)(4)} \sum_{l=0}^{5} Q\left(\hat{d}_l \sqrt{\frac{E_b}{N_0}} \right). \tag{52}$$

The modified distances for the first two terms are the same ones used in (50). The squared modified distances for the third term range from 0.58 to 0.59.

The performance of these two detectors is shown in Figure 13. Observe that the 32-state detector ($H = 3$, $p' = 8$, $L'' = 2$) has a loss of only 0.01 dB at $P_b = 10^{-5}$ and is the best 32-state detector analyzed in this paper. However, the 16-state detector ($H = 3$, $p' = 4$, $L'' = 2$) has a loss of 5 dB at $P_b = 10^{-5}$ and is by far the worst 16-state detector analyzed in this section. This has nothing to do with the orthogonal basis functions. (In fact, the same result occurs with $H = 64$.) The poor performance is

a result of the small modified distance associated with the rogue mergers. The rogue mergers introduce a distance loss of $10\log_{10}(1.29/0.59) = 3.4$ dB with respect to MLSD. The actual loss of 5.00 dB is much larger because of error propagation from the decision feedback. It is clear that the 16-state detector obtained by using RSSDα alone is a much better choice (see Table III).

V. SUMMARY AND CONCLUSIONS

The complexity/performance comparison between the combined methods described in Section IV is summarized in Table VIII. Note that the composite PAM detectors perform better than the composite frequency pulse truncation detectors as the state complexity goes down. The PAM approximation has the additional advantage of having fewer MFs. The 32-state detector based on the combination of orthogonal basis functions and RSSDθ with RSSDα is the best 32-sate detector in all categories. However the 16-state detector based on the same combination has the worst bit error rate performance.

In conclusion, it has been shown that there are two 32-state detectors whose loss in detection efficiency is less than 0.05 dB; two 16 state detectors whose loss in detection efficiency is less than 1 dB; and one 8 state detector whose loss in detection efficiency just greater than 1 dB. These complexity reductions were achieved by a proper *combination* of complexity reducing techniques. For a given state size, a combination of complexity-reducing techniques always outperforms the use of a single complexity-reducing technique, except when RSSDθ with RSSDα are applied too aggressively to the approximation based on orthogonal basis functions. The analysis and simulation results presented in this paper can be used to guide real implementations that strive to achieve a target complexity/performance goal.

REFERENCES

[1] T. Chalfant and C. Irving. Range telemetry improvement and modernization. In *Proceedings of the International Telemetering Conference*, pages 294 – 303, Las Vegas, NV, October 1997.

[2] W. Gao and K. Feher. FQPSK: A bandwidth and RF power efficient technology for telemetry applications. In *Proceedings of the International Telemetering Conference*, Las Vegas, NV, October 1997.

[3] T. Hill. An enhanced, constant envelope, interoperable shaped offset QPSK (SOQPSK) waveform for improved spectral efficiency. In *Proceedings of the International Telemetering Conference*, pages 127–136, San Diego, CA, October 2000.

[4] Range Commanders Council Telemetry Group, Range Commanders Council, White Sands Missile Range, New Mexico. *IRIG Standard 106-00: Telemetry Standards*, 2000. (Available on-line at http://jcs.mil/RCC/manuals/106-00).

[5] E. Law and K. Feher. FQPSK versus PCM/FM for aeronautical telemetry applications; spectral occupancy and bit error probability comparisons. In *Proceedings of the International Telemetering Conference*, pages 489–496, Las Vegas, NV, October 1997.

[6] T. Hill. Performance of SOQPSK and multi-h CPM in the presence of adjacent cahannel interference. In *Proceedings of the International Telemetering Conference*, pages 255–263, Las Vegas, NV, October 2001.

[7] J. B. Anderson, T. Aulin, C-E. Sundberg. *Digital Phase Modulation*. Plenum Press, New York, 1986.

[8] B. E. Rimoldi. "A decomposition approach to CPM". *IEEE Trans. Info. Theory*, 34:260–270, March 1988.

[9] A. Svensson, C-E. Sundberg, and T. Aulin. "A class of reduced-complexity Viterbi detectors for partial response continuous phase modulation". *IEEE Trans. Commun.*, 32:1079–1087, Oct. 1984.

[10] M. Geoghegan. Description and performance results for the advanced range telemetry (ARTM) Tier II waveform. In *Proceedings of the International Telemetering Conference*, San Diego, CA, October 2000.

[11] A. Svensson. "Reduced state sequence detection of partial response continuous phase modulation". *IEE Proc., pt. I*, 138:256–268, Aug. 1991.

[12] P. A. Laurent. "Exact and approximate construction of digital phase modulations by superposition of amplitude modulated pulses (AMP)". *IEEE Trans. Commun.*, 34:150–160, February 1986.

[13] U. Mengali and M. Morelli. "Decomposition of M-ary CPM signals into PAM waveforms". *IEEE Trans. Info. Theory*, 41:1265–1275, Sept. 1995.

[14] E. Perrins and M. Rice. "A linear PAM-based receiver for multi-h CPM". In *Proceedings of the International Telemetering Conference*, Las Vegas, NV, October 2003.

[15] E. Perrins and M. Rice. "PAM decomposition of M-ary multi-h CPM". *IEEE Transactions on Communications*, in review, September 2003.

[16] G. K. Kaleh. "Simple coherent receivers for partial response continuous phase modulation". *IEEE J. Select. Areas Commun.*, 7:1427–1436, Dec. 1989.

[17] G. Colavolpe and R. Raheli. "Reduced-complexity detection and phase synchronization of CPM signals". *IEEE Trans. on Commun.*, 45:1070–1079, Sept. 1997.

[18] E. Perrins and M. Rice. "Optimal and reduced complexity receivers for M-ary multi-h CPM". In *Proceedings of the IEEE Wireless Communications and Networking Conference, WCNC'04*, Atlanta, Georgia, March 2004.

[19] E. Perrins and M. Rice. Unified performance analysis of suboptimum detection methods for multi-h CPM. In *Proceedings of the IEEE Military Communications Conference*, Monterey, CA, October 2004.

[20] P. Moqvist and T. Aulin. "Orthogonalization by principal components applied to CPM". *IEEE Transactions on Communications*, 51:1838–1845, November 2003.

TABLE I

PARAMETERS DEFINING ARTM CPM.

symbol values	$\alpha_n \in \{-3, -1, +1, +3\}$
partial response	$L = 3$
frequency pulse	$f(t) = \begin{cases} \frac{1}{2LT}\left[1 - \cos\left(\frac{2\pi t}{LT}\right)\right] & 0 \le t \le LT \\ 0 & \text{otherwise} \end{cases}$
modulation indexes	$h_n \in \left\{\frac{4}{16}, \frac{5}{16}\right\}$

TABLE II

THE PERFORMANCE/COMPLEXITY TRADE-OFF FOR FREQUENCY PULSE TRUNCATION.

L'	number of states	number of MFs	loss (dB) at $P_b = 10^{-5}$
3	256	128	—
2	64	32	0.02
1	16	8	4.10

TABLE III

THE PERFORMANCE/COMPLEXITY TRADE-OFF FOR RSSDα.

L''	number of states	number of MFs	loss (dB) at $P_b = 10^{-5}$
3	256	128	—
2	64	128	0.07
1	16	128	2.00

TABLE IV

THE PERFORMANCE/COMPLEXITY TRADE-OFF FOR RSSDθ.

p'	number of states	number of MFs	loss (dB) at $P_b = 10^{-5}$
16	256	128	—
4	64	128	—
2	32	128	1.30

TABLE V

THE PERFORMANCE/COMPLEXITY TRADE-OFF FOR THE PAM APPROXIMATIONS.

Approximation	number of states	number of MFs[a]	loss (dB) at $P_b = 10^{-5}$
$K = 48$	256	128	—
$K = 12$	64	56	0.10
$K = 3$	16	20	1.95
$K = 1$	16	8	∞
$p_{k,i}(t)$	16	20	1.61
$\overline{g}_k(t)$	64	18	0.19

[a]This is the number of equivalent real-valued, length-T filters. This equivalent number is used to facilitate comparisons with the other techniques.

TABLE VI

THE PERFORMANCE/COMPLEXITY TRADE-OFF FOR THE ORTHOGONAL BASIS FUNCTION APPROXIMATION.

H	number of states	number of MFs	loss (dB) at $P_b = 10^{-5}$
64	256	128	—
3	256	12	0.01
3	256	8	0.15
3	256	4	2.20

TABLE VII

THE COMPLEXITY-REDUCTION PROPERTIES OF EACH PROPOSED TECHNIQUES.

approximation type	phase state reduction	correlative state reduction	MF reduction
pulse truncation		$\surd$	$\surd$
RSSDα		$\surd$	
RSSDθ	$\surd$		
PAM		$\surd$	$\surd$
basis functions			$\surd$

TABLE VIII

THE PERFORMANCE/COMPLEXITY TRADE-OFF FOR THE VARIOUS COMBINATIONS OF REDUCED-COMPLEXITY DETECTORS.

approximation	number of states	number of MFs	loss (dB) at $P_b = 10^{-5}$
MLSD	256	128	—
$L' = 8$, $p' = 8$	32	32	0.05
$L' = 4$, $p' = 8$	16	32	0.80
PAM-RSSDθ, $p' = 8$	32	18	0.08
PAM-RSSDθ, $p' = 4$	16	18	0.60
PAM-RSSDθ-RSSDα	8	18	1.05
$H = 3$, $p' = 8$, $L'' = 2$	32	12	0.01
$H = 3$, $p' = 4$, $L'' = 2$	16	12	5.00

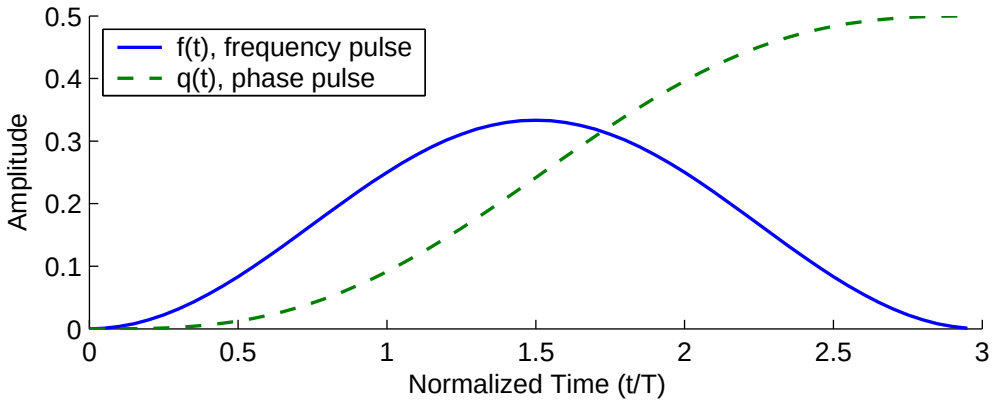

Fig. 1. The length-$3T$ raised cosine (3RC) frequency pulse and corresponding phase pulse for ARTM CPM.

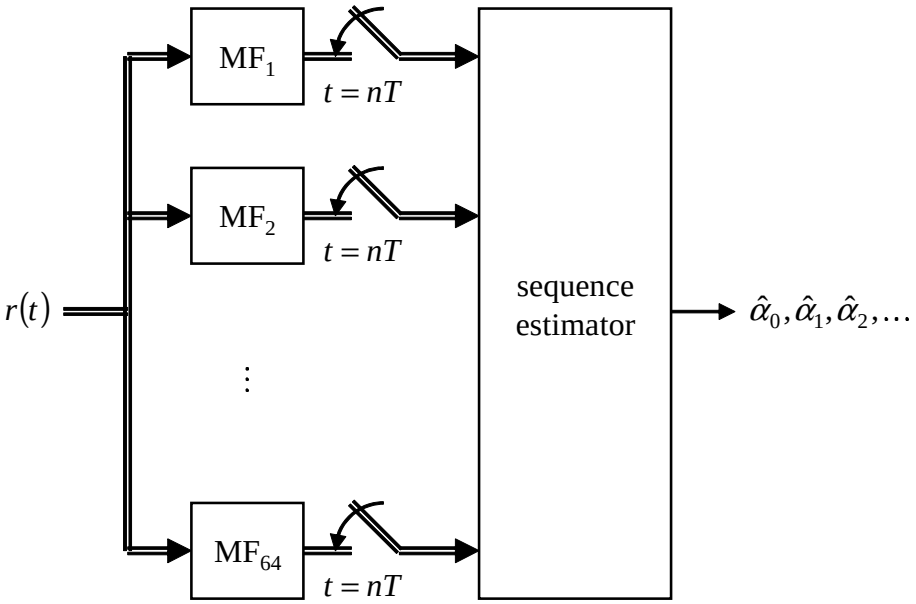

Fig. 2. CPM detector showing matched filters and the use of sampled matched filter outputs for sequence detection.

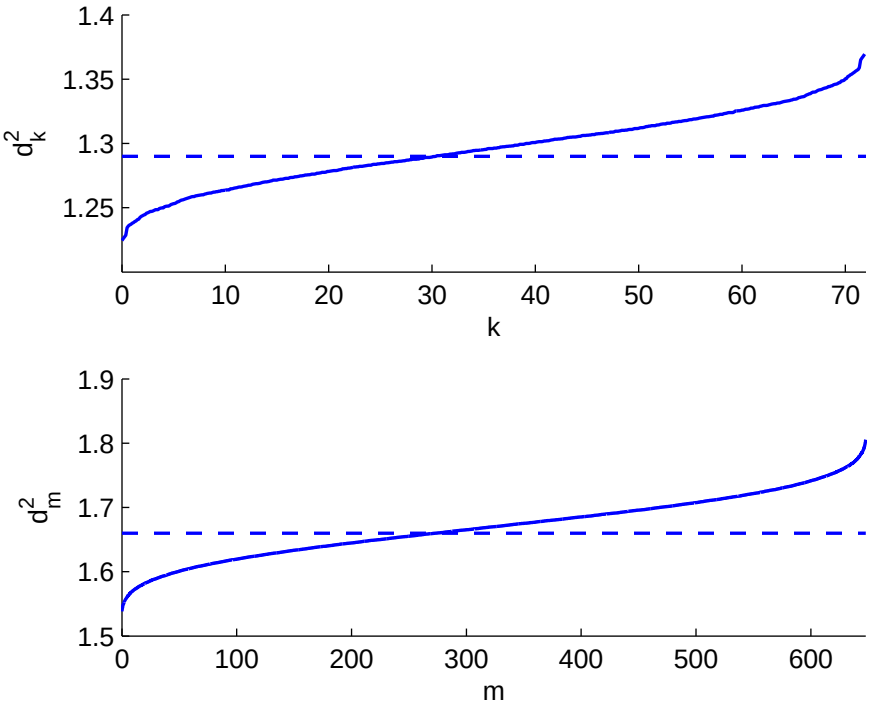

(a)

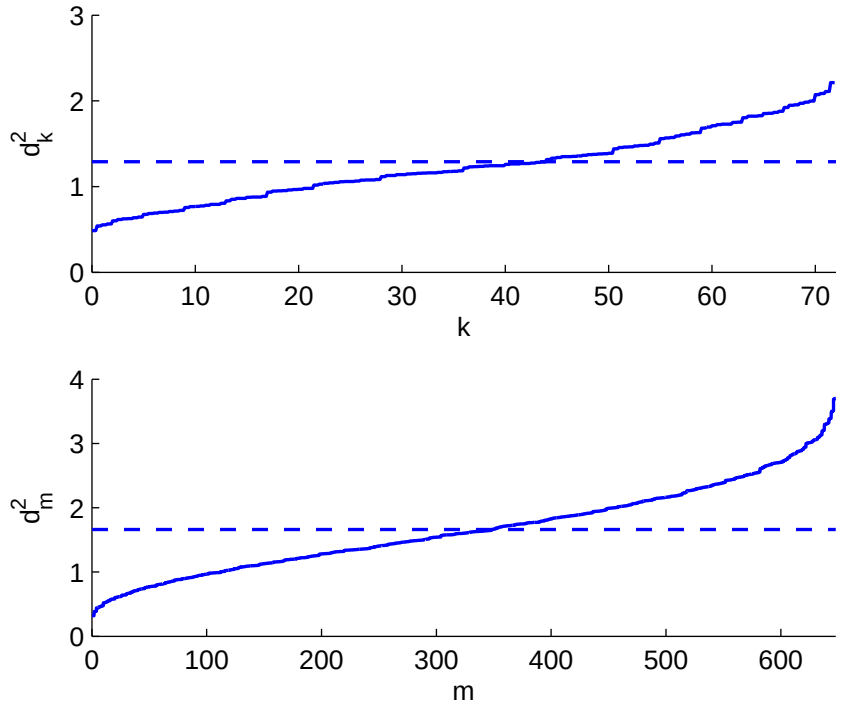

(b)

Fig. 3. Values of the squared distance for frequency pulse truncation with (a) $L' = 2$ and (b) $L' = 1$. These values are used in (23).

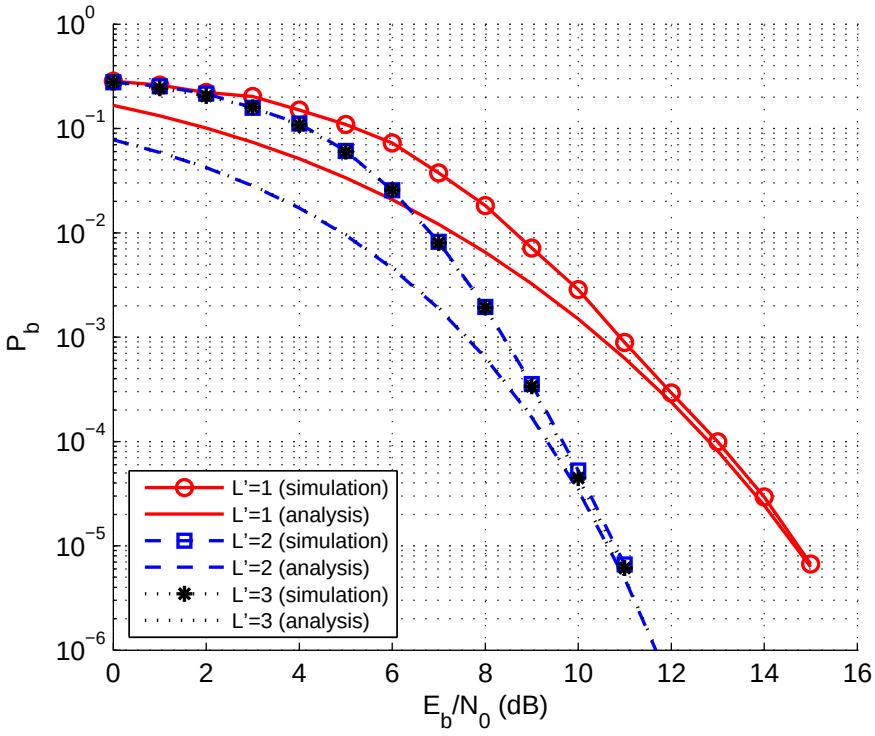

Fig. 4. The performance of detectors with frequency pulse truncation with $L' = 3$ (MLSD), $L' = 2$, and $L' = 1$.

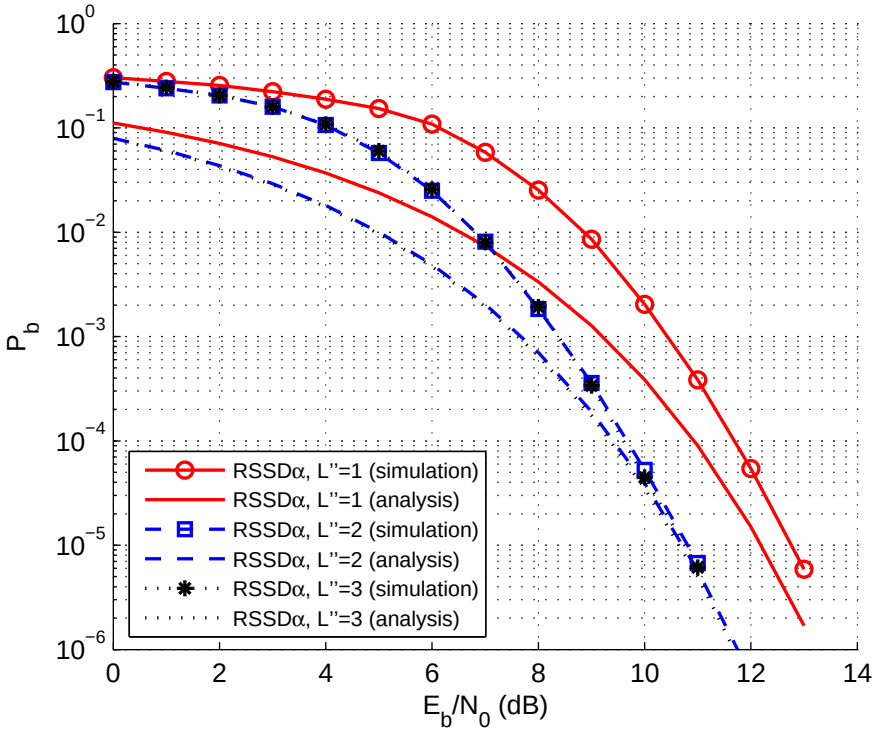

Fig. 5. The performance of RSSDα-type detectors with $L'' = 3$ (MLSD), $L'' = 2$, and $L'' = 1$.

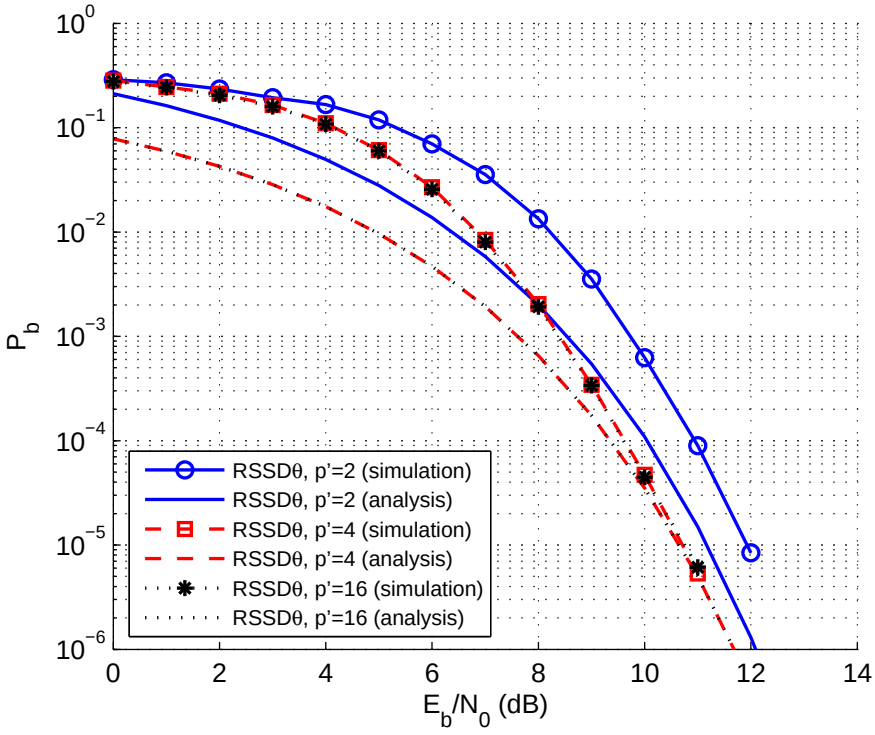

Fig. 6. The performance of RSSDθ-type detectors with $p' = 16$ (MLSD), $p' = 4$, and $p' = 2$.

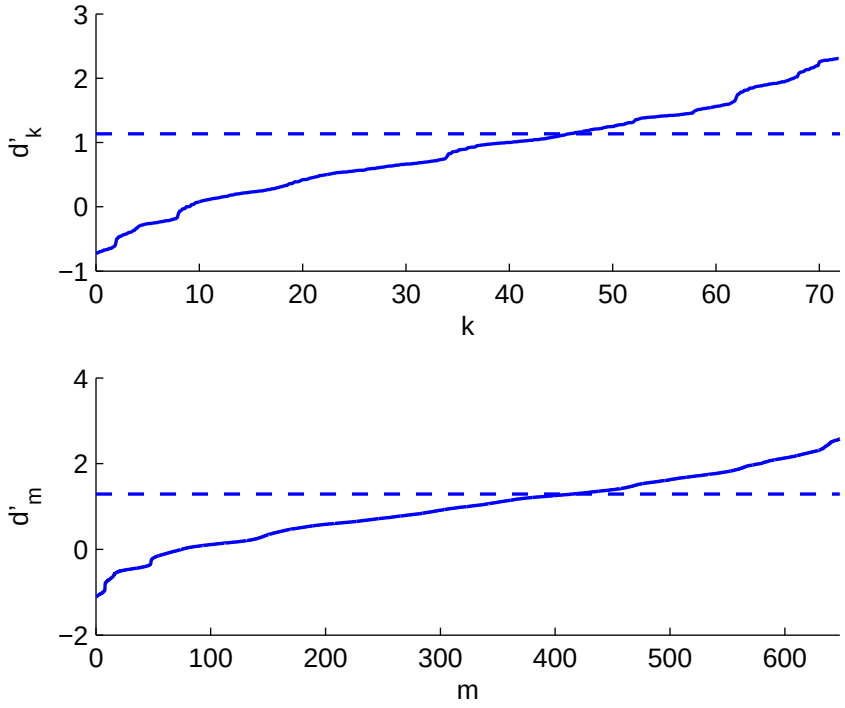

(a)

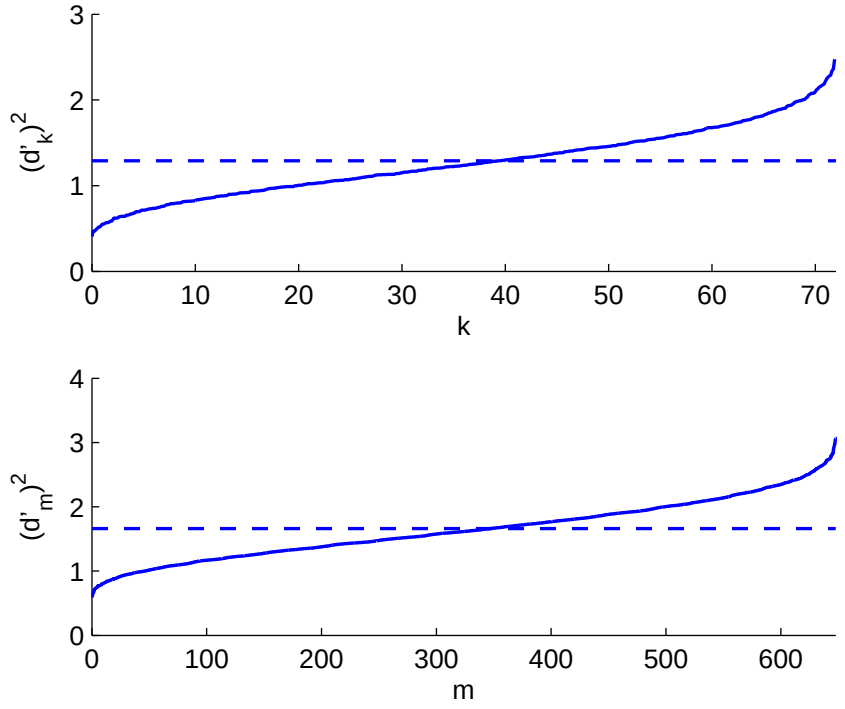

(b)

Fig. 7. (a) Values of the unsquared distance for the PAM approximation with $K = 1$. Note that some of these values are negative, which results in an error floor. (b) Values of the squared distance for the PAM approximation with $K = 3$.

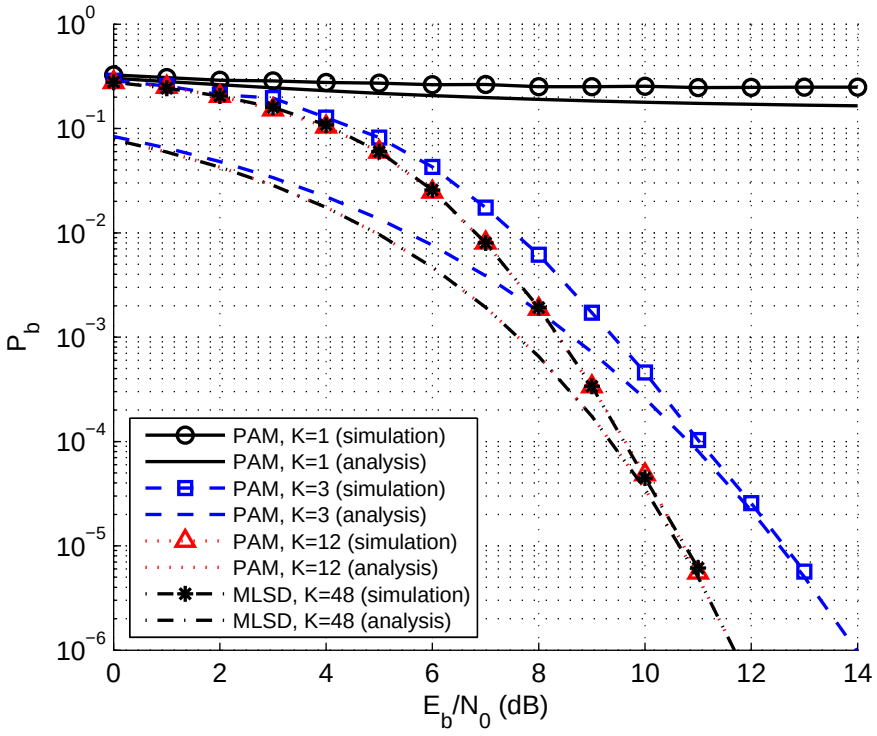

Fig. 8. The performance of PAM-type detectors with $K = 48$ (MLSD), $K = 12$, $K = 3$, and $K = 1$.

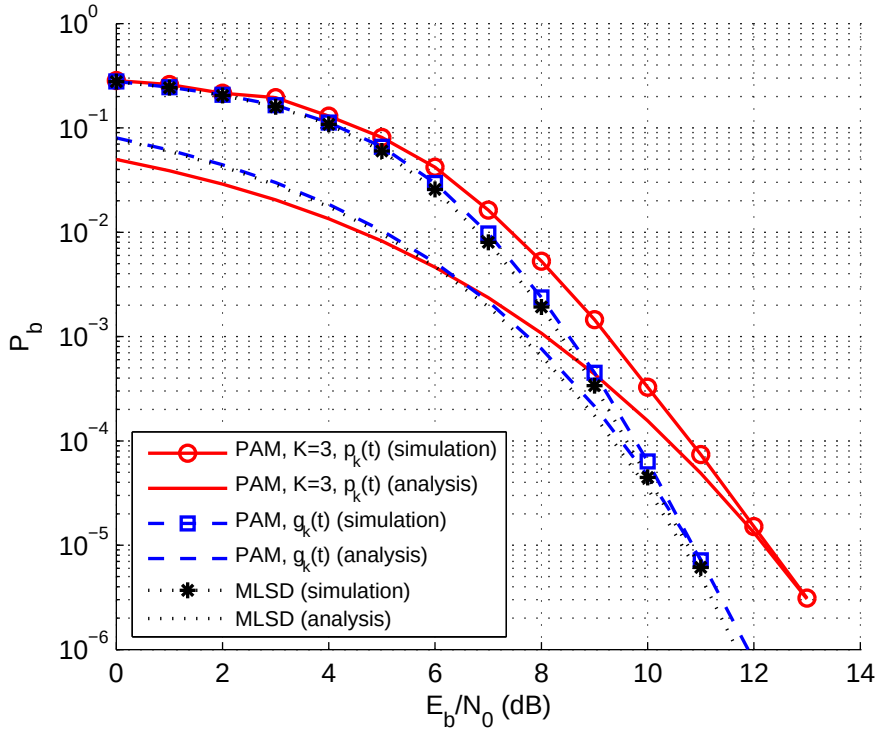

Fig. 9. The performance of PAM-type detectors with averaged pulses.

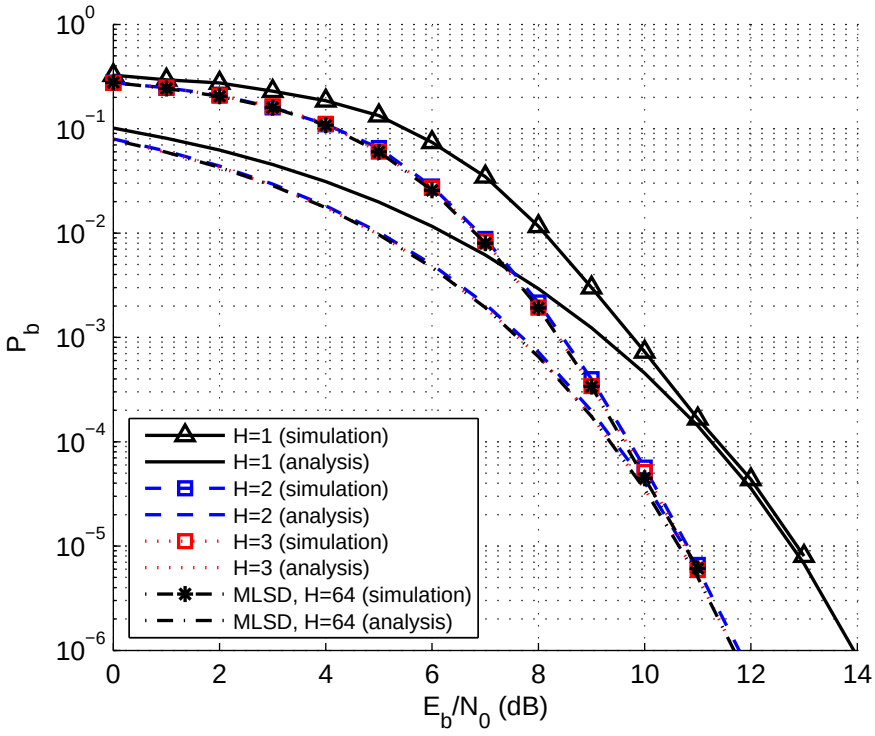

Fig. 10. The performance of detectors with orthogonal basis functions as MFs, where $H = 64$ (MLSD), $H = 3$, $H = 2$, and $H = 1$ basis functions are used.

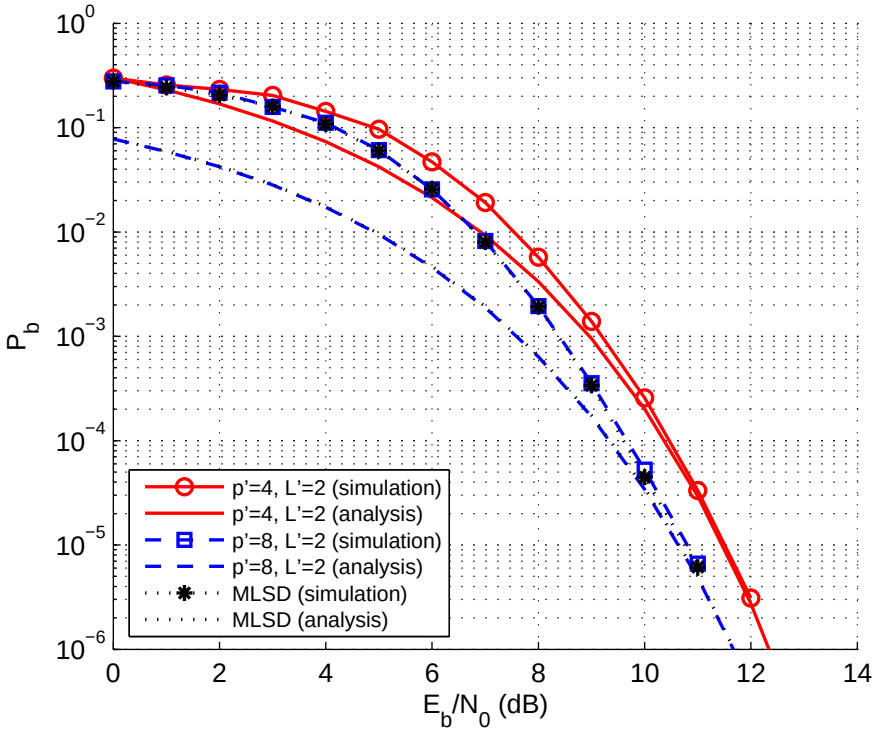

Fig. 11. Performance of detectors using a combination of frequency pulse truncation and RSSDθ.

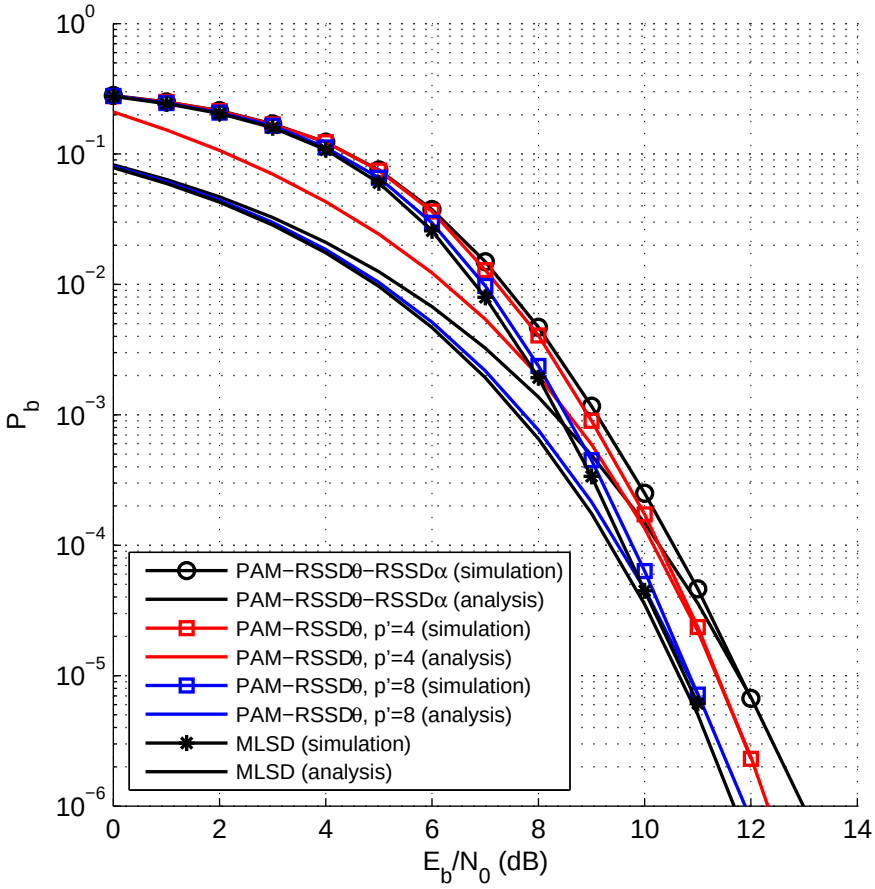

Fig. 12. Performance of detectors using a combination of PAM approximations, RSSDθ, and RSSDα.

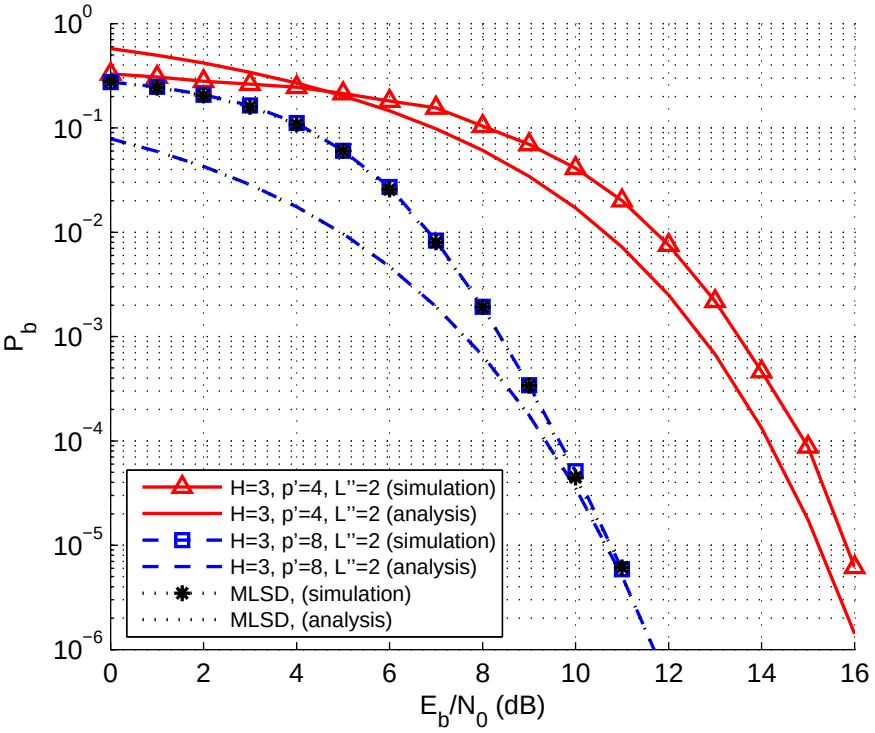

Fig. 13. Performance of detectors using a combination of orthogonal basis functions, RSSDθ, and RSSDα.